Seismic anisotropy of the Canadian High Arctic: Evidence from shear-wave splitting

Jean-Michel Dubé[a], Fiona A. Darbyshire[a,*], Mitch V. Liddell[b], Randell Stephenson[c], Gordon Oakey[d]

[a] Centre de recherche GEOTOP, Université du Québec à Montréal, CP 8888 succursale Centre-Ville, Montréal, QC H3C 3P8, Canada
[b] Department of Physics, CCIS, University of Alberta, Edmonton, AB T6G 2E1, Canada
[c] School of Geosciences, Geology and Geophysics, Meston Building, King's College, University of Aberdeen, Aberdeen AB24 3UE, UK
[d] Natural Resources Canada, 1 Challenger Drive, PO Box 1006, Dartmouth, Nova Scotia B2Y 4A2, Canada

ARTICLE INFO

ABSTRACT

The Canadian High Arctic preserves a long and complex tectonic history, including craton formation, multiple periods of orogenesis, extension and basin formation, and the development of a passive continental margin. We investigate the possible preservation of deformational structures throughout the High Arctic subcontinental lithosphere using measurements of seismic anisotropy from shear wave splitting at 11 seismograph stations across the region, including a N-S transect along Ellesmere Island. The majority of measurements indicate a fast-polarisation orientation that parallels tectonic trends and boundaries, suggesting that lithospheric deformation is the dominant source of seismic anisotropy in the High Arctic; however, a sub-lithospheric contribution cannot be ruled out. Beneath Resolute in the central Canadian Arctic, distinct back-azimuthal variations in splitting parameters can be explained by two anisotropic layers. The upper layer is oriented E–W and correlates with tectonic trends and the inferred lithospheric deformation history of the region. The lower layer has a ~NNE–SSW orientation and may arise from present-day convective mantle flow beneath locally-thinned continental lithosphere. In addition to inferences of anisotropic structure beneath the Canadian High Arctic, measurements from the far north of our study region suggest the presence of an anisotropic zone in the lowermost mantle beneath northwest Alaska.

1. Introduction

The Canadian Arctic is a geologically complex region with a tectonic history spanning over 2 billion years from the Archean to the Cenozoic. It forms a significant part of the margin of the as-yet poorly understood Arctic Ocean, and has been affected by numerous episodes of orogenesis, rifting and basin formation (e.g. Pease et al., 2014). In this paper we explore the potential roles of lithospheric deformation and present-day sublithospheric (convective) mantle flow in the tectonic evolution of the Canadian High Arctic. Such processes typically create fabrics that display different seismic velocities depending on the direction of wave propagation. We study these anisotropic structures using observations of shear wave splitting.

1.1. Geological setting

The oldest rocks in the Canadian High Arctic study area (Fig. 1) are

those of the Archean-Proterozoic Laurentian proto-continent, now exposed in the Greenland-Canadian Shield. These crystalline basement rocks are overlain by Mesoproterozoic clastic sediments in the southern part of the study area as well as younger Arctic Platform sediments. Later, up to 8 km of sediments were deposited on the northern Laurentian passive margin between the Neoproterozoic and Devonian, collectively known as the Franklinian Basin (Fig. 1). The Franklinian Basin comprises the Franklinian Shelf and deeper-water Hazen Trough successions (e.g. Oakey and Chalmers, 2012; Piepjohn and von Gosen, 2018; Stephenson et al., 2018, and references therein).

The Franklinian successions, exposed only on Ellesmere Island in the study area, have been strongly affected by deformation during the Ellesmerian Orogeny, as has the Pearya Terrane, which is generally considered to be an extraneous continental fragment of non-Laurentian origin, accreted northern Laurentian margin during the orogeny (e.g. Trettin et al., 1991; Piepjohn and von Gosen, 2018; c.f. Hadlari et al., 2014). Ellesmerian orogenesis terminated by the latest Devonian -

---

* Corresponding author.
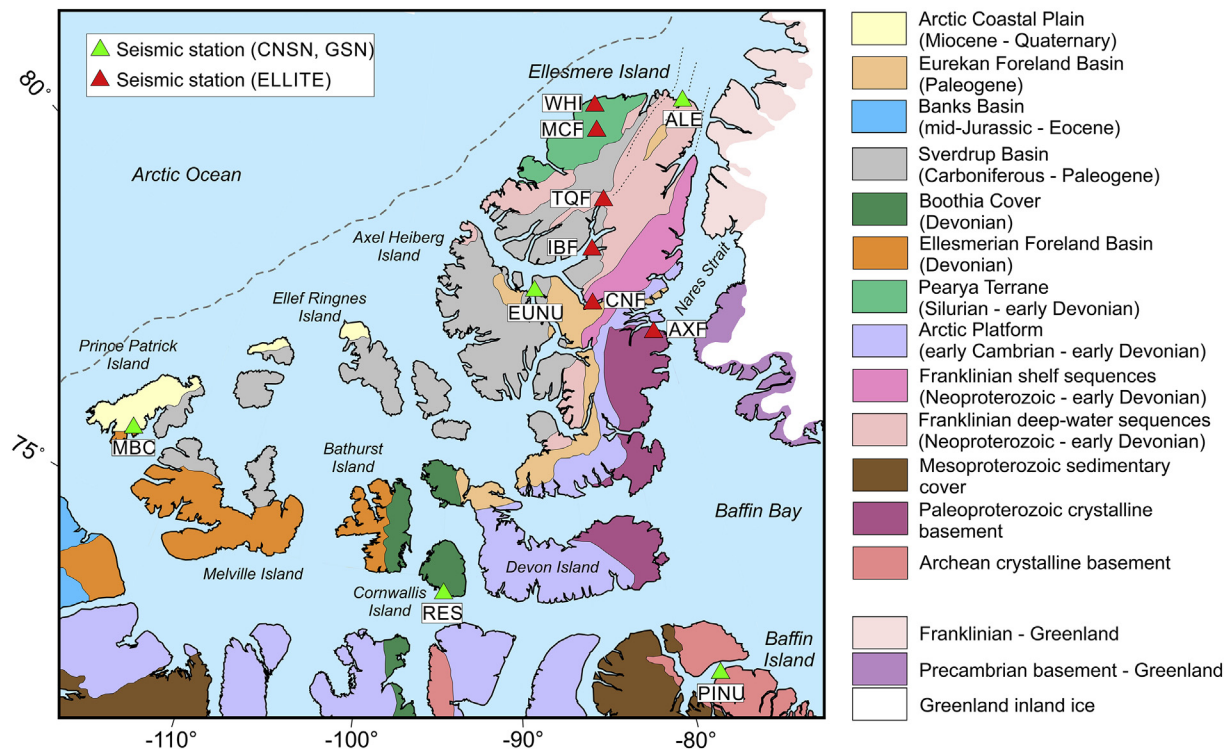 *E-mail address:* darbyshire.fiona_ann@uqam.ca (F.A. Darbyshire).

Fig. 1. Geological-tectonic map of the Canadian High Arctic, simplified from Oakey and Stephenson (2008); Harrison et al. (2011); St-Onge et al. (2015), showing seismic stations used in this study. The dashed grey line marks the approximate location of the continental shelf edge.

earliest Carboniferous and created a 400 km wide and > 3000 km long fold-and-thrust belt along the Arctic margin of North America. It is mostly covered in the study area by the sediments of the younger Sverdrup Basin although the Devonian-aged foreland basin of the Ellesmerian Orogeny is exposed to the southwest of the Sverdrup Basin.

The Sverdrup Basin developed over much of the Canadian Arctic Archipelago from the Carboniferous to the Paleogene, with a maximum sedimentary thickness estimated to be ~13 km (Embry and Beauchamp, 2008). Strata in the eastern part of the Sverdrup Basin, especially on Axel Heiberg and Ellesmere Islands, as well as some of the older Pearyan and Franklinian strata on Ellesmere Island, were compressionally and transpressionally deformed during the intraplate Eurekan Orogeny in the Paleogene. This deformation was caused by relative motions between Greenland and the NE Canadian Arctic during the early opening of the North Atlantic and Eurasian Arctic oceans (e.g., Piepjohn and von Gosen, 2018).

1.2. Previous geophysical studies

Various seismic methods have been used to study the crustal architecture of the Canadian High Arctic region, including sedimentary basin thickness and the thickness of the crystalline crust. Surface wave studies (e.g. Brune and Dorman, 1963; Wickens and Pec, 1968; Wickens, 1971) provided information on path-averaged structures across the region, whereas active-source refraction-reflection studies provided detailed information along a number of 2D profiles across Baffin Bay, Nares Strait, the Sverdrup Basin and the Arctic continental margin (e.g. Buchbinder, 1963; Keen et al., 1972; Jackson et al., 1977; Forsyth et al., 1979; Asudeh et al., 1989; Argyle and Forsyth, 1994; Forsyth et al., 1994, 1998; Reid and Jackson, 1997; Jackson and Reid, 1994; Jackson et al., 1998; Funck et al., 2006, 2011). They found crustal thicknesses ranging from 22 to 30 km close to the continental margins to 34–42 km further inland in the Arctic. Receiver function studies by Darbyshire (2003); Dahl-Jensen et al. (2003) gave Moho depth estimates from 25 to 32 km at the northern tip of Ellesmere Island

to 33–37 km elsewhere in the High Arctic. Schiffer et al. (2016) analysed receiver functions along a north-south profile on Ellesmere Island, finding a large range of Moho depths from 29 to 32 km at the edge of the Sverdrup Basin to 45–48 km beneath parts of the Central Ellesmere Domain.

Crustal architecture has also been studied using gravity modelling, notably for the region of Ellesmere Island and the NE Arctic (e.g. Oakey and Stephenson, 2008; Schiffer and Stephenson, 2018; Stephenson et al., 2018). Moho depths are generally in close agreement to those constrained by seismic imaging (both refraction and receiver function), and such studies provide important complementary information to measure crustal structure on a regional scale.

Upper-mantle seismic velocity structure and lithospheric thickness have been studied through surface-wave and full-waveform analysis at regional, continental and global scale (e.g. Darbyshire, 2005; Bedle and van der Lee, 2009; Yuan et al., 2011; Schaeffer and Lebedev, 2014; Lebedev et al., 2018). High shear wave velocities, consistent with cratonic lithosphere, extend beneath most of the Canadian High Arctic to at least 200 km depth with the exception of Baffin Bay, where the lithosphere has been thinned by rifting, and the central Sverdrup Basin region, where the lithospheric thickness is closer to ~150 km.

Seismic anisotropy beneath the Canadian High Arctic has been studied through SKS splitting measurements for the sparse network of Canadian permanent seismic stations (Helffrich et al., 1994; Bostock and Cassidy, 1995; Silver, 1996; Barruol et al., 1997; Evans et al., 2006, e.g.). Further information about upper-mantle anisotropy can be gained from global surface wave tomography (e.g. Becker et al., 2012; Debayle and Ricard, 2013; Yuan and Beghein, 2013; Schaeffer et al., 2016); however the lateral resolution of the models is generally low and there is little agreement between them for the northernmost latitudes.

While aeromagnetic and gravity maps can provide useful information on tectonic boundaries and large-scale crustal structure, correlation between the anomaly patterns and those of lithospheric-scale seismic anisotropy is uncertain. However, in the case of stable continental lithosphere, Curie depths (the maximum depth of remnant rock

magnetism, controlled by temperature) may extend into the upper lithospheric mantle, and correspondence between seismic anisotropy patterns and potential-field data has been used to argue for crust-mantle tectonic coupling (e.g. Bokelmann and Wüstefeld, 2009). Bouguer gravity anomalies in central and northern Ellesmere Island parallel the main tectonic trends with a roughly NE-SW orientation (Oakey and Stephenson, 2008; Gaina et al., 2014; Petrov et al., 2016). Magnetic anomaly trends have been mapped in detail across much of the Canadian Arctic; however the data set is incomplete, notably for the northern Ellesmere Island region.

1.3. Seismic anisotropy and shear wave splitting

Core-refracted shear waves are often used to measure seismic anisotropy because the P-to-S conversions at the core-mantle boundary erase all source-side anisotropy, and the S phase is thus initially radially polarised when it exits the core on the receiver side (e.g. Savage, 1999). When the shear wave encounters an anisotropic medium - generally presumed to lie in the upper mantle - it will split, creating two orthogonally-polarised quasi-shear waves. The quasi-shear wave orientated along the fast-polarisation orientation ϕ of anisotropy travels faster in the medium than the other phase, which is orientated perpendicular to the anisotropy, creating a delay time δt between the two phases which is measurable at the receiver. The presence of anisotropy and the resulting shear wave splitting results in energy on the tangential-component seismogram, together with an elliptical particle motion arising from the delay time between the quasi-shear phases.

The two measured parameters, ϕ and δt, provide valuable information about past and present geodynamics. The fast-polarisation orientation is most typically related to lithospheric deformation, which may give rise to aligned structural and/or mineralogical fabrics, to the direction of sublithospheric convective mantle flow, or to a combination of these sources. Delay time is controlled by both the thickness of the anisotropic layer and the strength of its anisotropy.

2. Data acquisition

Our data set consists of 11 broadband seismic stations distributed across the Canadian High Arctic (Fig. 1, Table 1). 5 are permanent or long-term installations with recording periods between 7 and 29 years, affiliated to the Global Seismograph Network (GSN) or Canadian National Seismograph Network (CNSN). In addition, we use data recorded between 2010 and 2012 by 6 temporary stations of the Ellesmere Island Lithospheric Experiment (ELLITE; Stephenson et al. (2013); Schiffer et al. (2016)). The method used to measure seismic anisotropy uses core-refracted shear waves (SKS, SKKS and PKS, hereafter referred to generally as XKS); in order to acquire the relevant data we initially searched for earthquakes of magnitude ≥ 6.0 at epicentral distances of $\geq 88°$ from the stations (or, in the case of the more closely-spaced

Table 1
Seismograph stations used in this study. GSN: Global Seismic Network, CNSN: Canadian National Seismograph Network, ELLITE: Ellesmere Island Lithospheric Experiment.

Affiliation	Station	Latitude	Longitude	Operation
GSN	ALE	82.50	−62.35	02/1990-present
CNSN	EUNU	80.05	−86.42	08/2000-present
CNSN	MBC	76.32	−119.36	08/1992–06/1997
CNSN	PINU	72.70	−77.98	09/2000–12/2007
CNSN	RES	74.69	−94.90	02/1992-present
ELLITE	AXF	78.88	−75.78	06/2010–06/2011
ELLITE	CNF	79.66	−80.78	06/2010–08/2012
ELLITE	IBFE	80.61	−79.58	06/2010–08/2012
ELLITE	MCF	82.65	−75.04	06/2010–08/2012
ELLITE	TQF	81.41	−76.85	06/2010–08/2012
ELLITE	WHI	83.09	−74.15	06/2010–08/2012

ELLITE stations, from the central point of the network, close to station IBFE). The data were bandpass filtered between 0.04 and 0.3 Hz to enhance the signal-to-noise ratio of the XKS phases, and careful visual quality control was used to select the highest-quality data for further analysis. Data quality is defined by a combination of high signal to noise ratio, a stable waveform free of artefacts, and clear XKS phases that are well separated in time from each other and from direct S or Sdiff arrivals. Following data quality control, we checked the seismograms for their specific XKS content, i.e. the occurrence of PKS, SKSac/df and SKKS phases, as each phase occurs at a characteristic epicentral distance range. While some seismograms only had one phase of sufficient quality for splitting measurements, others had two, e.g. SKS/SKKS or PKS/SKKS, and were separated accordingly.

3. Methodology

3.1. Shear wave splitting measurements

We measured the shear wave splitting parameters using a variation of the approach of Silver and Chan (1991). This method uses a grid search over physically-plausible values of ϕ and δt to find the combination that best minimises the second eigenvalue of the particle motion matrix in the chosen analysis window, equivalent to linearising the particle motion. To do this, the horizontal components are rotated and one component is time-shifted in the analysis window, until the waveforms match. We use the analysis method of Teanby et al. (2004) in which measurements are made over a number of different analysis windows - in our case, 100 - followed by a cluster analysis which finds the most stable splitting parameters, analyses errors and estimates the source polarisation using the eigenvalues of the particle-motion matrix.

Shear wave splitting measurements can generally be described by two categories (Fig. 2). A 'split' shows energy on the tangential component, an elliptical particle motion, and a well-defined ϕ and δt measurement resulting from the analysis. In contrast, a 'null' is characterised by an initial particle motion that is already linear, and there is no energy on the tangential component. In the case of a null, the value of ϕ has a 90° ambiguity and the value of δt is undefined. Null results can potentially arise from three possible situations: the passage of the shear wave through an azimuthally-isotropic medium, the cancelling of multiple layers of anisotropy beneath the station, or an earthquake backazimuth parallel or perpendicular to the fast-polarisation orientation of anisotropy.

We checked the results for significant difference between event backazimuth and estimated source polarisation. Backazimuth is the angular direction between the source and the receiver, while the source polarisation is the actual direction from which the incoming earthquake energy was observed. These directions are typically close together, as the shear wave is radially polarised when it exits the core. Possible explanations for differences between source polarisation and backazimuth include polarisation filter artefacts (e.g. Hammond et al., 2005), complex deep mantle anisotropy (e.g. Restivo and Helffrich, 2006), a mixing of phases that arrive at nearly the same time, or sensor misalignment (e.g. Walpole et al., 2014). Anomalies may also come from small-scale anisotropic structures in the mantle that could bend the XKS wave and thus change the apparent arrival direction (e.g. Jenkins et al., 2017). Our data set does not exhibit consistent anomalies at any particular station, which would indicate sensor misalignment, nor any systematic correlations with particular backazimuth ranges, which might allow some constraint on the causes of the anomalies. We therefore believe it better to remove measurements exhibiting such anomalies (a small subset) from our data set. Following Walpole et al. (2014), we removed any measurement with a backazimuth - source polarisation anomaly greater than 15°.

For the long-term (GSN and CNSN) stations with a large number of measurements, we stacked the splitting results for each station in order to make an initial estimation of the dominant fast-polarisation
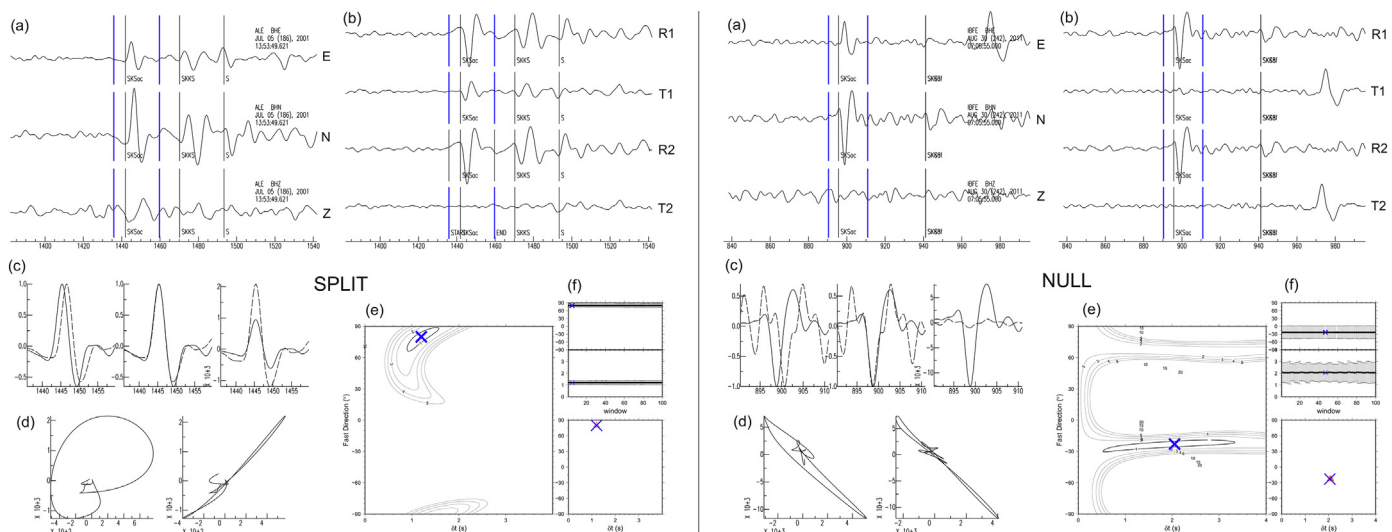
Fig. 2. Examples of shear-wave splitting measurements. Left: a 'split', Right: a 'null'. (a) Original 3-component seismogram with shear phases marked; the blue lines show the limits of the analysis window. (b) Radial and tangential components before (R1, T1) and after (R2, T2) correction for splitting. (c) Zoom into the analysis window. The first panel shows the fast and slow waveforms after rotation but before correction for δt, the second shows the corrected aligned waveforms scaled to each waveform's maximum amplitude and the third shows the same waveforms with absolute amplitude. (d) Particle-motion plot before (left) and after (right) correction. (e) Contour plot showing the optimal combination of ϕ and δt. (f) Results of individual measurements from each of the 100 windows analysed. (For interpretation of the references to colour in this figure legend, the reader is referred to the web version of this article.)

orientation of anisotropy at each station prior to more detailed analyses. The stacking procedure is based on the method of Restivo and Helffrich (1999) which is a modification of that of Wolfe and Silver (1998). The entire misfit distribution over the ϕ-δt grid search for each measurement is summed for the ensemble of measurements, allowing both splits and nulls to be incorporated into the stack. The stack is also weighted for signal-to-noise ratio and scaled according to how well-sampled a given backazimuth range is.

3.2. Modelling for multiple anisotropic layers

We carry out further modelling of our observed data, using a first-order class archetype to guide the procedure. The three most basic possible models are a single anisotropic layer, two anisotropic layers, and a single dipping layer. Each of these predicts a distinctive pattern of backazimuthal variation in splitting parameters. A single layer will not vary as a function of backzimuth, a dipping anisotropic layer will vary smoothly with roughly 360° periodicity, and a two-layer model will include sharp jumps and have a roughly 90° periodicity (Fig. 3; Silver and Savage, 1994). While these models are simplified, it is important to note that sharp jumps in splitting parameters are not possible for
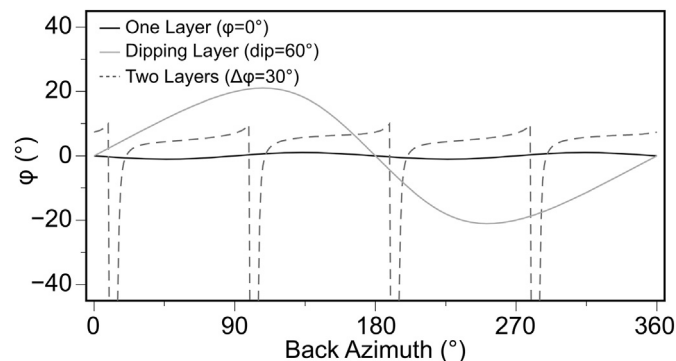
Fig. 3. Synthetic ϕ responses for three basic classes of anisotropy. $\Delta\phi$ indicates difference in fast-polarisation orientation between layers. Layer thickness and alignment fraction of olivine a-axis can change delay time, but does not affect the backazimuth patterns. Modified from Liddell et al. (2017).

dipping or single layers, and their observation is therefore diagnostic of a multi-layer anisotropic system.

The chosen model class should be the simplest possible that can explain the observations. In many data sets, even when results exhibit some systematic variations in splitting parameters, the backazimuthal coverage is insufficient to interpret anything other than a single, horizontal anisotropic layer with a single pair of splitting parameters representing the effective anisotropy of the medium beneath the station.

Where splitting parameters suggest a pattern consistent with that predicted for a two-layered anisotropy regime (e.g. Savage, 1999), we used the MSAT toolkit of Walker and Wookey (2012) to search for a combination of two anisotropic layers that could explain the backazimuthal variations.

Modelling proceeded via a grid search of possible anisotropic orientations from 0° to 180°, advancing by 5°, in an upper and lower layer. Grid search results were calculated for both ϕ and δt. Layer thickness and fractional alignment of olivine can affect the magnitude of delay time, but this was not included because our intention is to minimize degrees of freedom in the model, and those parameters do not affect the backazimuthal pattern of splitting parameters, which is more diagnostic. Similar modelling of multiple and dipping layer models has been performed successfully in this region previously by Liddell et al. (2017). The search proceeds by creating a synthetic model for a given combination of parameters and computing an RMS misfit between these synthetic data and the observations for station RES. The RMS was calculated using Eq. (1).

$$RMS = \sqrt{\frac{1}{n}(x_1^2 + x_2^2...x_n^2)}$$

(1)

for n observed data points and x difference between each data point and the modelled curve. Nulls are not included in this calculation because they have no fixed single ϕ value and δt is undefined. Thus they cannot be directly compared to the model response. We performed a parallel analysis whereby null measurements were converted into equivalent split measurements with ϕ defined as perpendicular to the backazimuth (this aligned closer to the true observations) and large errors on δt values such that they did not contribute to fits. Including nulls in this way made almost no difference to the model result, so we feel it is better to limit our models and analysis only to splits. We included an
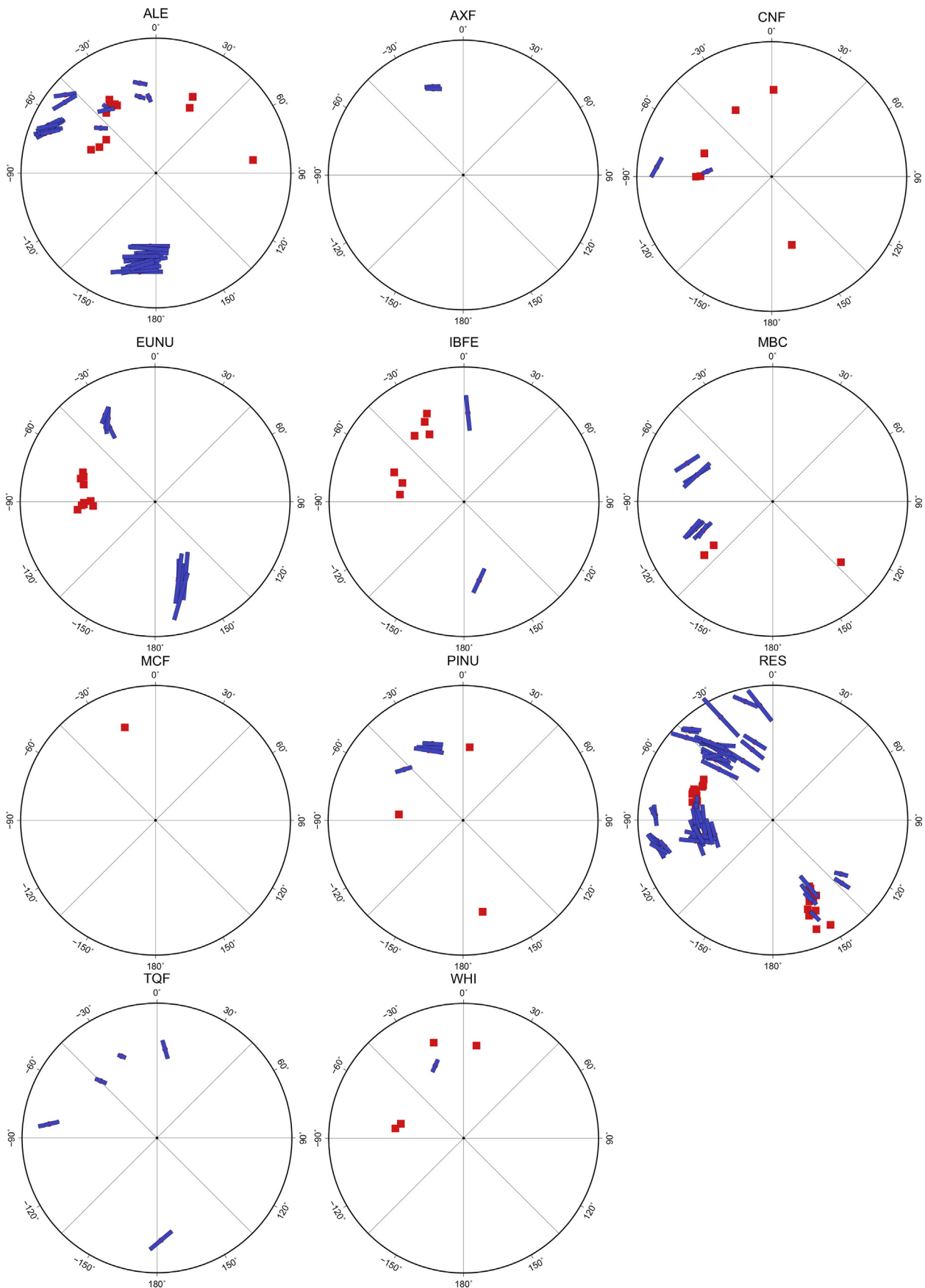
Fig. 4. Polar plots showing splits (blue bars) and nulls (red squares) for each of the stations analysed. The backazimuth of the incident earthquake is plotted clockwise from North (0°) and the radius is proportional to the incident angle of the incoming XKS wave. (For interpretation of the references to colour in this figure legend, the reader is referred to the web version of this article.)
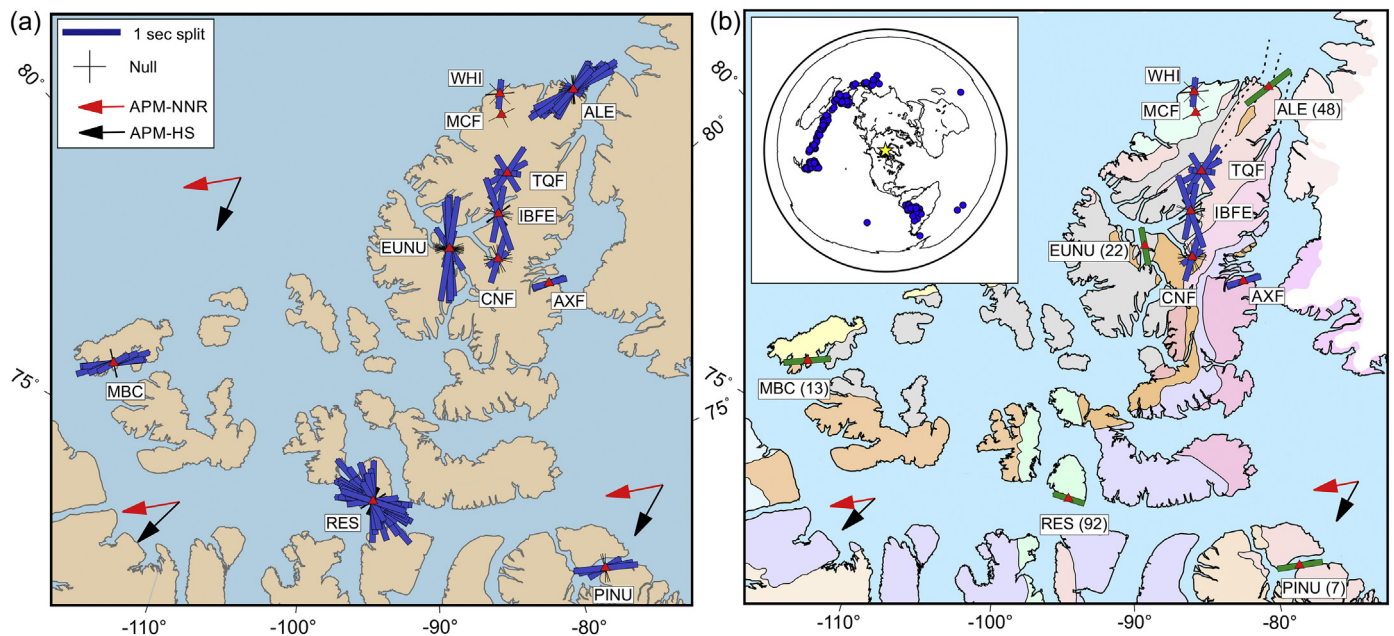
Fig. 5. Compilation of shear wave splitting measurements on a map of the High Arctic. (a) Individual measurements; blue bars denote high-quality splits and black crosses denote high-quality nulls. (b) Composite of individual measurements at ELLITE stations (blue bars, crosses) and stacked splits at CNSN/GSN stations (green bars); the number of measurements per stack is given in parentheses. Inset: earthquakes (blue circles) used in this study; the yellow star marks the centre of the study area. APM: absolute plate motion. NNR: no-net-rotation reference frame (e.g. Argus et al., 2010); HS: Pacific hotspot reference frame (e.g Gripp and Gordon, 2002). (For interpretation of the references to colour in this figure legend, the reader is referred to the web version of this article.)

error estimate of ± 5° for the backazimuth of the observed data when calculating RMS misfit with the modelled results. After computing an RMS value for each combination in the grid search, the model parameters that produce the lowest RMS can be picked out. The absolute value of the RMS misfit is less important in this case than the existence of a clear global minimum region in the grid, so the values were normalized to 1.

4. Results

4.1. Shear wave splitting measurements

Figs. 4 and 5a show the full set of results for our data set. A limited number of measurements is available for the ELLITE stations due to their short recording time, and station PINU, which was noisier than the other long-term installations, also provided a limited set. The longest-running stations, ALE and RES, yielded 48 and 92 high-quality measurements respectively, allowing for more detailed analysis not only of the dominant fast-polarisation orientation but of its backazimuthal variation.

The majority of splits for stations ALE, EUNU, PINU and MBC cluster relatively closely around a dominant fast-polarisation orientation: NE–SW, N-S, E–W and ENE-WSW respectively. In contrast, we observe significant variation in fast-polarisation orientation at station RES, with a mean ~NW–SE fast-polarisation orientation. In Fig. 5b, splits are stacked for the long-term stations. In the stacked results (Table 2), we observe a consistent fast-polarisation orientation for ALE, EUNU, MBC and PINU with that inferred from the individual result sets; however the dominant fast-polarisation orientation for RES is closer to WNW–ESE than the NW–SE mean inferred visually from the individual results.

Delay times for individual splits average ~0.66 s for the ELLITE stations, with individual values ranging from 0.33 to 0.98 s. Mean values for the long-term stations are consistently higher (0.9–1.1 s), though with more internal variability due to the larger data sets and better azimuthal coverage.

From north to south, the ELLITE stations exhibit varying splitting parameters. WHI has a NNE fast-polarisation orientation for the single

Table 2
Stacked splits for the 5 long-term GSN/CNSN stations. Previous results from Helffrich et al. (1994); Bostock and Cassidy (1995); Silver (1996); Barruol et al. (1997); Evans et al. (2006). ϕ: Fast-polarisation orientation; δt: Delay time.

Station	ϕ (°)	δt (s)	No. measurements	Previous results (ϕ, δt)
ALE	83 ± 0.75	0.98 ± 0.03	48	61–82°, 0.91–1.25
EUNU	−4 ± 1.75	0.68 ± 0.08	22	–
MBC	63 ± 2.25	0.73 ± 0.10	14	43°, 0.85
PINU	−84 ± 1.50	0.80 ± 0.04	7	–
RES	−74 ± 0.75	0.58 ± 0.01	92	−60°, 0.95–1.64

measured split, with a cluster of nulls in the N and E backazimuth quadrants. MCF has a single null measurement with a NNW–SSE (or WSW–ENE) orientation. TQF splits vary between NNW–SSE and NE–SW in fast-polarisation orientation, depending on event backazimuth, suggesting that a more complex structure than a single horizontal anisotropic layer is needed to explain the measurements; however the sparse data set does not allow us to discriminate between multiple layers versus a single dipping layer. The fast-polarisation orientations at IBFE are broadly similar to those at EUNU, with a similarly large delay time. At CNF, two splits are measured, from western backazimuths, showing a NE–SW fast-polarisation orientation, and nulls are measured in the NW and SE quadrants. AXF has two clear splits, with E–W fast-polarisation orientations.

For stations ALE and RES, the number of individual measurements is high enough to allow a more detailed inspection of backazimuthal variation. Fig. 6 shows the variation of ϕ and δt as a function of earthquake backazimuth. Although the azimuthal coverage is by no means complete, being restricted to a limited southern cluster plus a wider W to NNE swath, we observe significant variation in splitting parameters with backazimuth. This observation suggests that the initial stacked single-layer estimate does not reflect the true anisotropic structure beneath these stations, and that at least two different anisotropic layers are instead contributing to the shear wave splitting measurements.
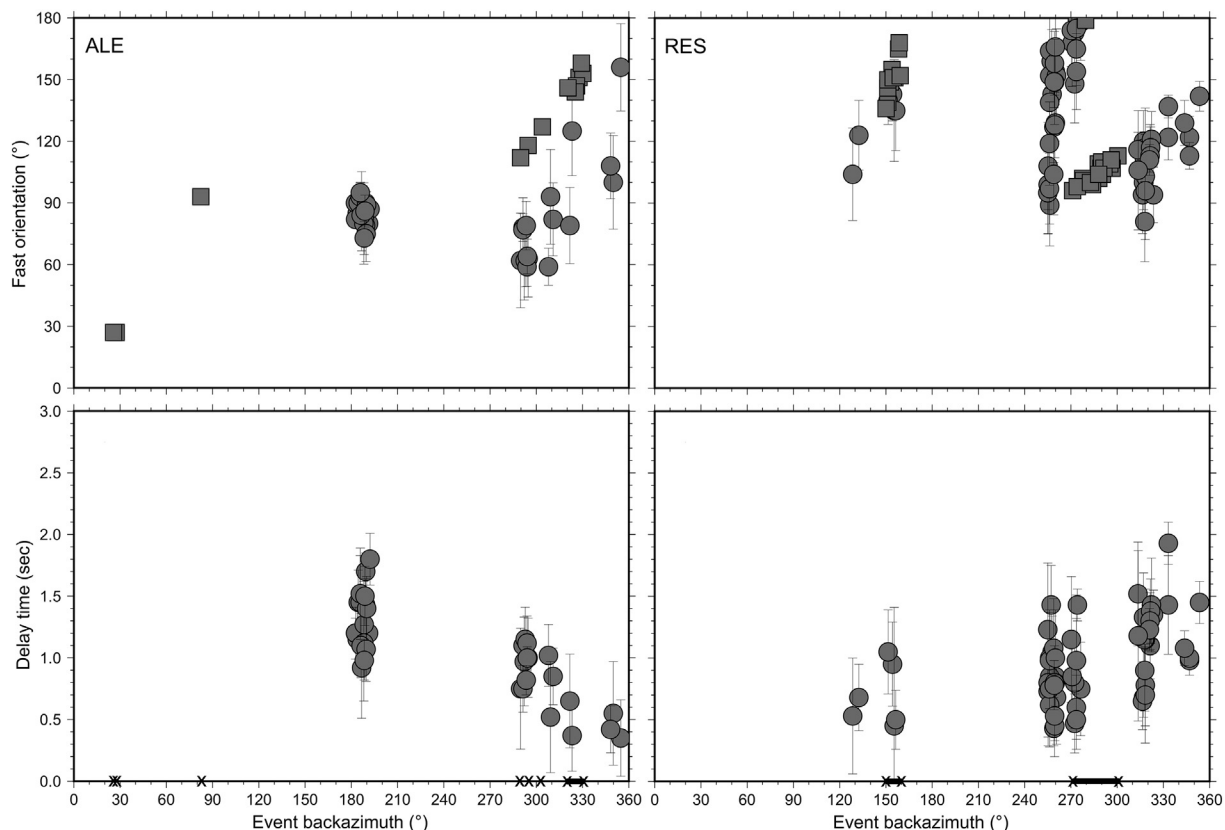
Fig. 6. Backazimuthal variation of splitting measurements at stations ALE and RES. Splits are shown in both graphs as circles with error bars; nulls are shown as squares in the fast-polarisation orientation graph. Delay time is undefined for a null measurement; the positions of the nulls are indicated at zero delay time by an 'X'. For ease of plotting, all fast-polarisation orientations are expressed in the 0–180° range.
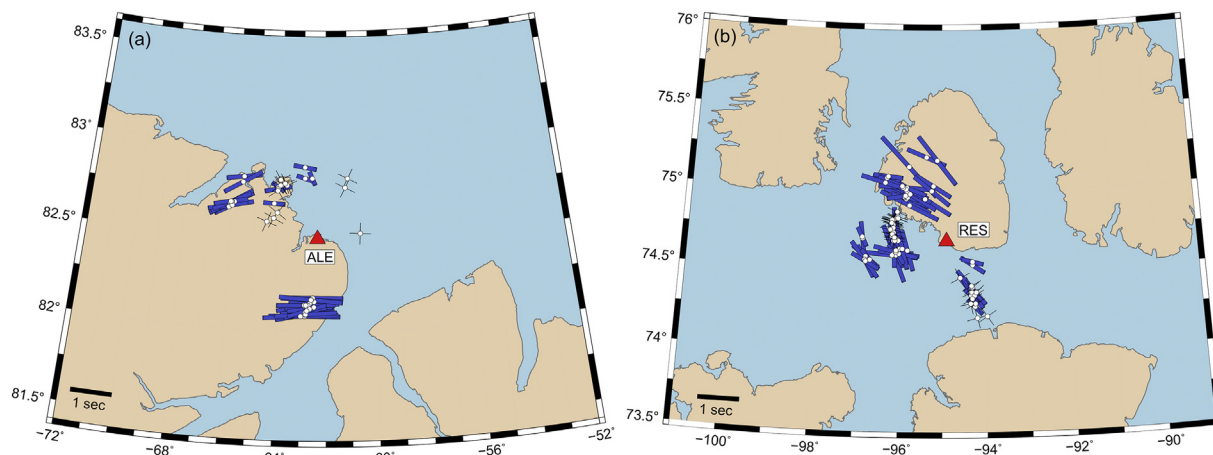

Fig. 7. Spatial variation of splitting measurements at stations ALE and RES, shown as bars (splits) and crosses (nulls) at coordinates corresponding to the ray's piercing point at 200 km depth beneath the station.

The azimuthal distribution of splitting measurements at these two stations is also visualised by maps (Fig. 7) in which each measurement is plotted at the piercing point of the ray at 200 km depth, using a standard global reference model (IASP91; Kennett and Engdahl (1991)) to calculate an approximate ray geometry. The ray trajectories and corresponding piercing points are determined using the TauP Toolkit of Crotwell et al. (1999).

ALE shows a high degree of consistency between results for earthquakes at similar azimuth and ray parameter; all southern events give splits of δt > 1 s with a consistent E–W orientation. Smaller-magnitude splits are found to the north of the station and nulls dominate in the NE

quadrant. In the WNW and NW, we observe a clear discrepancy between splitting parameters at larger incidence angles and those at smaller incidence angles. The larger incidence angles are associated with SKKS arrivals, and exhibit delay times of ~0.7–1.2 s, whereas the smaller incidence angles, associated with SKS arrivals, exhibit either null characteristics or splits with small delay times that are close to null in character.

The results for RES are more complicated, with both azimuth and ray parameter appearing to play a role. Delay times in the NW quadrant are consistently > 1 s with a NW–SE fast-polarisation orientation. There are two distinct clusters of nulls in the SSE and WNW quadrants, a
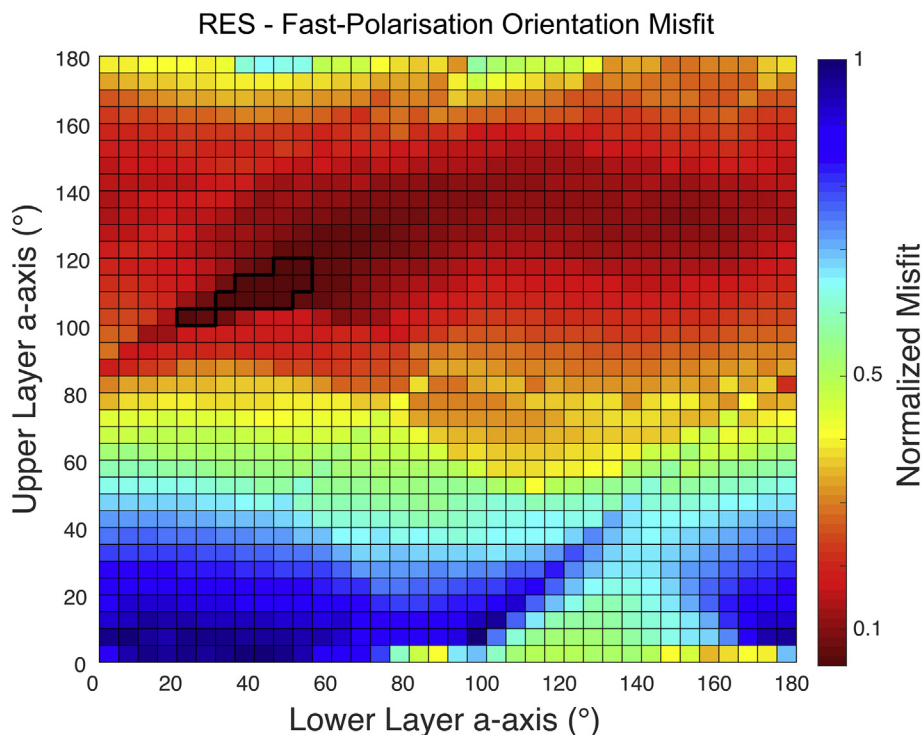
Fig. 8. Normalized RMS misfit surface for ϕ at station RES. Lowest misfit is achieved for a relatively small subset of possible model orientations. The black outline indicates where models have the lowest RMS misfit.

subset of splits in the SSE for the most distant earthquakes (piercing points closest to the station) and small ($\delta t < 1$ s) splits to the WSW with more variable fast-polarisation orientations.

4.2. Multiple anisotropic layers at station RES

The results of the MSAT search for combinations of two anisotropic layers beneath station RES are shown in Fig. 8. Each cell is coloured by the normalized RMS misfit value. The fast-polarisation orientation grid search result is, to first order, divided in half; the best fitting models have a generally SE/NW oriented layer above a NE/SW layer. There is also a clear region with the lowest RMS values in the upper left portion of the grid. The delay time grid search result has no clear region of lowest misfit, and cannot constrain any preferred model. The lowest RMS error found by the MSAT grid-search algorithm suggests an upper layer with a fast-polarisation orientation of 105° and lower layer with fast-polarisation orientation of 30°. However, a better visual fit to the data is achieved by changing the anisotropy orientations slightly to 90° and 30° for the upper and lower layers, respectively (Fig. 9). This model was found by perturbing the minimum-RMS model to determine its sensitivity to small changes in layer fast-polarisation orientations. The "visual fit" model still lies within the low-RMS zone indicated by the black outline in Fig. 8. This discrepancy of 15° likely lies both within the errors inherent in the original splitting measurements and in the simplifying assumptions made in the modelling process. The significant misfit discrepancy between the grid search minimum and the better visual fit lies in the highly-variable fast-polarisation orientations for the western backazimuths (~250–270°). At this backazimuth there are mathematically two different "correct" fast-polarisation orientations at the top and bottom of the sharp jump: ~170° and ~90°. Any observed split will naturally be more or less influenced by one or the other end of that system due to small perturbations away from the ideal synthetic scenario. We therefore suggest that, while the grid search minimum model has the lowest RMS misfit, the "visual fit" model might better reflect reality. This model provides a possible explanation for the large spread in fast-polarisation orientations over such a small backazimuth

window (~250–270°). The two models differ by only 15° in upper-layer fast-polarisation orientation, and both positively identify a two-layered system as the best model to explain the data. It is also interesting to note the close alignment of the diamonds representing null measurements in the synthetic model near 160° and 270°–300° backazimuth (Fig. 9). As discussed in Section 3.1, null measurements can be due to the back-azimuth of the incoming earthquake aligning either parallel or per-pendicular to the effective anisotropic fast-polarisation orientation of the medium. The wave may split multiple times, but constitutes a single observation that includes information about the cumulative effect of all layers of the Earth beneath the station. It is by observing patterns in the backazimuthal variation of splitting parameters that we can investigate whether there are multiple layers of anisotropy. It seems most likely that sources from these backazimuths happen to arrive perpendicular to the direction they would otherwise report as the fast-polarisation or-ientation, simply by chance. A roughly E–W oriented anisotropy in the upper layer and NNE/NE–SSW/SW orientation in the lower layer ap-pears to provide an adequate explanation for the measurements at station RES.

5. Discussion

Arctic Canada has a long history of orogenesis, rifting and basin formation, but is at present considered a stable continental platform. Seismic anisotropy across the region is therefore most likely to arise from "fossil" fabrics preserved in the lithosphere following large-scale deformation, structural alignments of tectonic boundaries, shearing at the base of the lithosphere associated with plate motion, present-day sublithospheric mantle convective flow, or some combination of these factors. Below we examine the possible causes of Arctic seismic aniso-tropy in the context of our splitting measurements.

5.1. Potential sources of seismic anisotropy

• *Crustal contributions.* Previous studies of seismic anisotropy (e.g. Barruol and Mainprice, 1993; Silver, 1996) suggest that the maximum
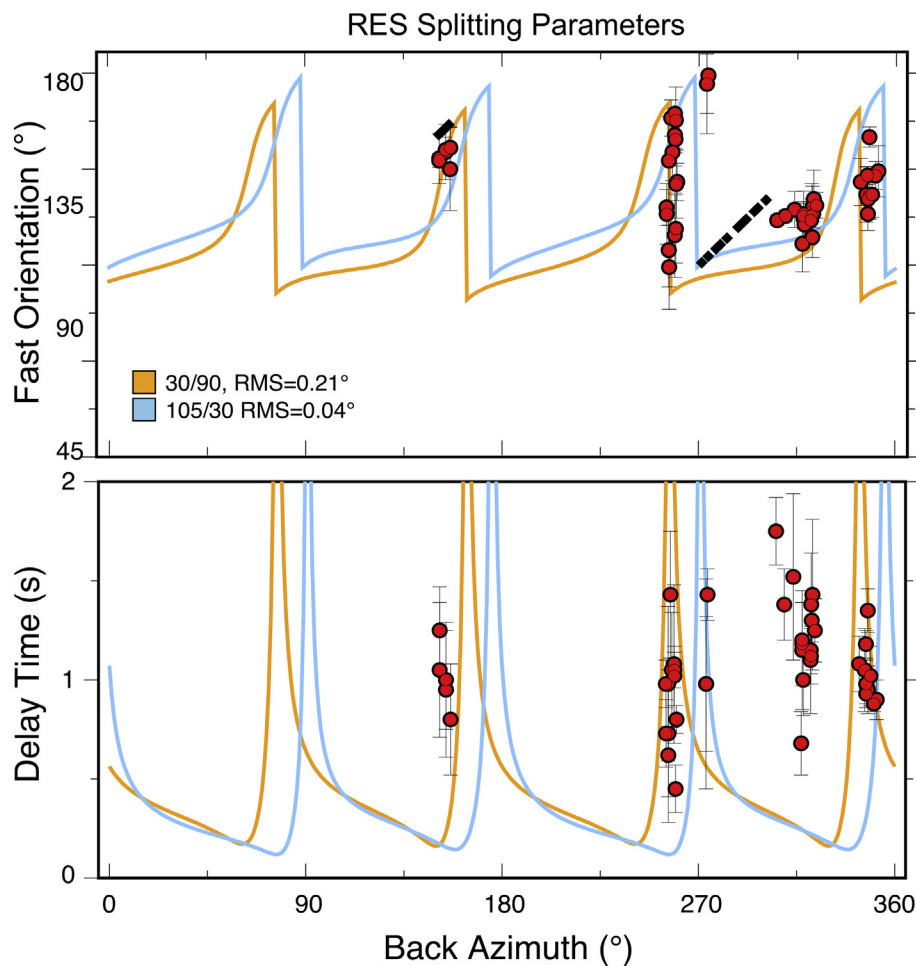
Fig. 9. Best-fitting models for two-layered anisotropy at station RES. Diamonds indicate null measurements and are placed as if backazimuth is parallel to equivalent fast-polarisation orientation. Note that the data have error bars in both X and Y, but those in X are too small to be visible compared to the size of the plotted data point.

contribution of continental crust to the shear wave delay time is ~0.3–0.5 s. We therefore compare the delay times obtained in this study to ascertain whether an anisotropic crust is sufficient to explain our observations, or whether a mantle component is necessary.

• *Lithospheric deformation and tectonic boundaries*. It is possible to attribute lithospheric anisotropy to "fossil" deformation arising from past strain, which acts to align intrinsically anisotropic minerals such as olivine. One way to infer such fabric is to compare the fast-polarisation orientations of shear wave splitting measurements with surface tectonic boundaries which may indicate zones of lithospheric deformation such as rifting, shear and orogenesis. Such a comparison makes the assumption that deformation is vertically coherent between the crust and the lithospheric mantle (e.g. Silver and Chan, 1988, 1991). The hypothesis has previously been used to explore the link between XKS splitting observations and structures such as major orogenic belts, e.g. the Appalachian and Trans-Hudson orogens in North America (e.g. Bastow et al., 2011; Long et al., 2016).

• *Plate motion and basal shear*. Shear wave splitting fast-polarisation orientations are often compared to "absolute" plate motion (APM), which is thought to give rise to basal drag from interaction between the moving plate and the sublithospheric mantle. However, these comparisons should be made with a certain degree of caution, because the APM directions inferred from the NNR (No Net Rotation, e.g. Argus et al., 2010) and HS (Pacific hotspot, e.g. Gripp and Gordon, 2002) can often be significantly different. In addition, the development of basal drag fabric is thought to be affected by plate velocity (e.g. Debayle and Ricard, 2013), with slow-moving plates unable to generate a basal drag

fabric strong enough to create significant anisotropy.

• *Active mantle convective flow*. Strain associated with mantle flow is generally thought to cause the alignment of olivine *a* axes in the flow direction, and the resulting crystallographic-preferred orientation (CPO) will thus give rise to a significant anisotropic fabric (e.g. Zhang and Karato, 1995; Bystricky et al., 2000; Tommasi et al., 2000; Kaminski and Ribe, 2002). In general, the olivine CPO will be rotated towards the infinite strain axis associated with active mantle convective flow in the asthenosphere and below due to simple shear (e.g. Conrad et al., 2007).

• *Lower-mantle anisotropy*. The lowermost mantle and D″ layer have been shown to be anisotropic, though this phenomenon is not ubiquitous (e.g. Nowacki et al., 2011, and references therein). Lower mantle anisotropy may be visible in shear wave splitting as a systematic discrepancy in splitting parameters (ϕ and δt, or splits versus nulls) between SKS and SKKS arrivals coming from events in the same region. These arrivals have very similar paths and Fresnel zones in the upper mantle, but sample the lowermost mantle significantly differently due to their ray paths.

A challenge when considering the relative contributions of lithospheric and sublithospheric anisotropy is the lack of direct depth constraint inherent to XKS measurements. For each individual measurement, the observed splitting parameters represent the integration of the entire path from core to receiver. We can, however, indirectly infer relative depth by considering the effect of lateral heterogeneity in anisotropy on the measurements made at closely-spaced stations, using the width and overlap of the XKS Fresnel zones (e.g. Alsina and Snieder,
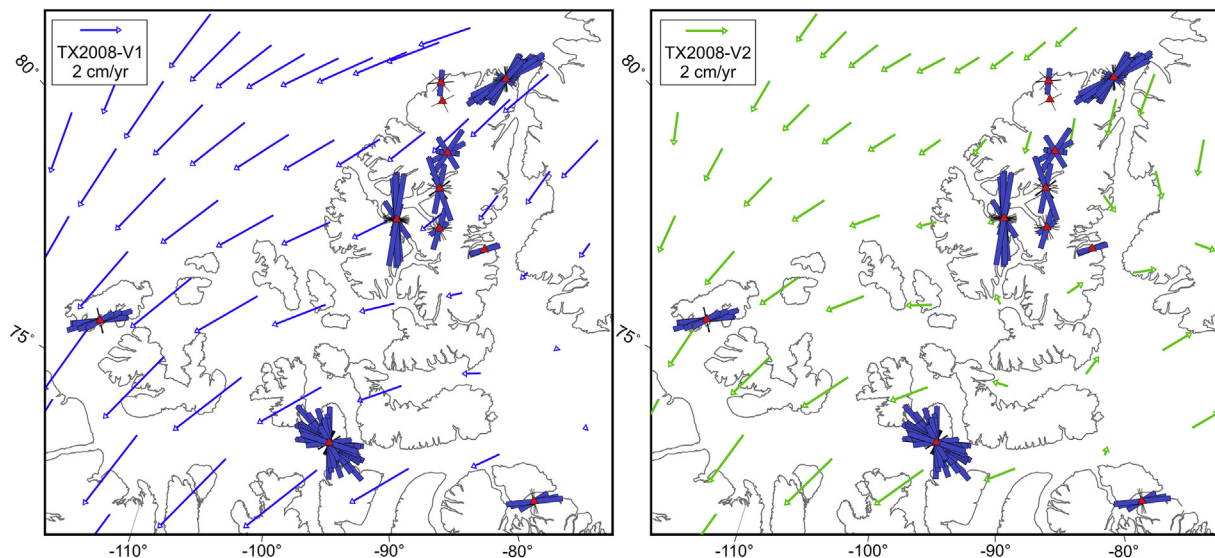
Fig. 10. Splitting results from Fig. 5 superimposed on two models of the sublithospheric mantle flow field, based on two radial viscosity profiles V1 and V2.

1995). Sublithospheric mantle flow is expected to vary laterally on a scale that would lead to very gradual variations in splitting parameters between closely-spaced stations, whereas the smaller scale of lateral heterogeneity in lithospheric anisotropy could result in significant lateral variation of splitting parameters at these stations (e.g. Savage, 1999; Bastow et al., 2007, 2011; Liddell et al., 2017). We can therefore make a preliminary estimation of the relative depth of anisotropic heterogeneities beneath Ellesmere Island by considering the similarities and differences between the splitting parameters measured at ALE, the ELLITE stations, and EUNU.

5.2. Thickness of anisotropic layers

Based on the ensemble of delay times for the stations in our study region, we can estimate to first order the corresponding thickness of the anisotropic layer (assuming, for simplicity, a single layer that gives rise to the effective anisotropy measured). The maximum delay times or individual events are of the order 1.5 s. This would suggest a thickness of ~170–350 km, based on the relationship $L \simeq \delta t \overline{V_s}/dV_s$ (Helffrich, 1995), if we assume an average anisotropy strength of 2–4% (e.g. Savage, 1999; Ben-Ismail et al., 2001). For a delay time of 0.5 s, estimated layer thicknesses using the same parameters lie in the range ~60–115 km. Recent tomography models (Schaeffer and Lebedev, 2014; Lebedev et al., 2018) suggest that the lithosphere underlying our study region is of the order ~150–250 km thick, with the exception of the area below station RES, where shear wave velocity profiles suggest a thickness of ≤150 km.

Based on layer thickness considerations alone, an anisotropic contribution uniquely from the lithosphere or the sublithospheric mantle could be plausible for the smaller delay times. However, for the majority of stations across the study area, the larger observed delay times suggest that contributions from both sources would be required to explain the inferred layer thicknesses.

5.3. Tectonic boundaries in the Canadian High Arctic

The variability of the ELLITE splitting measurements over short spatial scales (Fig. 5), together with the backazimuthal variation apparent at stations ALE and RES (Fig. 6), suggest that lithospheric fabric plays a strong role in the development of seismic anisotropy for the High Arctic region. For most of the stations analysed, many of the delay times are too large to be attributed only to the crust. Mean splits at different stations vary from 0.55 to 1.25 s, with the smallest values

suggestive of either weak anisotropy or a relatively thin anisotropic layer where the crust could be a significant contributor. Dominant fast-polarisation orientations at many of the Ellesmere Island stations, as well as Baffin Island station PINU, parallel the main tectonic trends visible at the surface. Lithospheric structural trends are more difficult to identify at MBC due to the deposits of continental-shelf sediments on the northern half of Prince Patrick Island. Station WHI in northern Ellesmere Island lies within the Pearya terrane, and its single split precludes a reliable comparison with surface tectonics. Station RES, on southern Cornwallis Island, lies at the intersection of several surface-tectonic features, including the N-S Boothia trends and E–W striking fold belts. The Sverdrup Basin lies to the north, and large-scale tectonics associated with its formation may have produced lithospheric deformation beyond the basin margins, but this is uncertain. RES exhibits complex splitting parameters including evidence for layered anisotropy, and will be discussed in more detail in Section 5.5.

5.4. Plate motion versus mantle flow

In the Canadian High Arctic, direct comparison between fast-polarisation orientations and "absolute" plate motion (APM) is complicated by the significant difference between the plate motion directions in the NNR and HS reference frames, which can reach over 60°. A subset of stations (Fig. 5) exhibits fast-polarisation orientations approximately parallel to NNR-APM and others appear subparallel to HS-APM, but there is no region-wide correlation. In addition, the slow APM speed (~17–23 mm/y) of the North American plate in this region lies well below the threshold of 40 mm/yr proposed by Debayle and Ricard (2013) for the development of basal drag fabric related to APM, and we therefore discount this phenomenon as a significant contribution to our observations.

In order to assess the possible contributions from active mantle convective flow, we compare the ensemble of fast-polarisation orientations across our study region with the horizontal components of the mantle flow field predicted by Forte et al. (2015) from a global seismic-geodynamic tomography model (Fig. 10). The mantle flow predictions are made for two different radial viscosity profiles: V1 (Mitrovica and Forte, 2004) has a 100 km thick high-viscosity lithospheric layer whereas for V2 (Forte et al., 2010) the high-viscosity layer is 200 km thick, similar to that of average cratonic lithosphere. We note that, although flow directions vary across the region, the flow field varies more smoothly than the variations in anisotropy, even for the large station spacings outside Ellesmere Island. We observe a few

possible local-scale correlations between the mantle convective flow directions and fast-polarisation orientations (e.g. V1 with the PINU stack and the principal splits at ALE); however the deviations across much of our study region are large. Our observations suggest that, even though it may contribute to the anisotropy measured in the High Arctic, mantle convective flow is unlikely to be the dominant factor.

5.5. Complex anisotropy

The shear wave splitting measurements at EUNU, MBC and PINU are consistent with a simple interpretation of a single layer of anisotropy with a horizontal axis, as fast-polarisation orientations do not vary significantly with backazimuth (Fig. 4). Stations AXF, CNF, IBFE, MCF and WHI are ambiguous, as the sparse nature of the data set does not allow us to distinguish between a simple anisotropy versus a more complicated pattern. In contrast, more complex anisotropy is inferred for stations ALE, RES and TQF. In the case of ALE, much of the variation is linked to SKS/SKKS discrepancy, and is described in more detail below. However, we also note that this station lies very close to a set of NW–SE trending tectonic boundaries in northern Ellesmere Island (Fig. 5b). It is possible that the XKS waves may sample different lithospheric blocks according to event backazimuth, and this may contribute to the variations in splitting parameters. Station TQF exhibits distinct and significant backazimuthal variation, suggesting that either a dipping layer or multiple layers would be necessary to characterise the anisotropy beneath this station. Due to the limited data set, we cannot distinguish unambiguously between these two classes. The fast-polarisation orientation appears to vary smoothly between 180° and 340° backazimuth, similar to a dipping-layer prediction (Fig. 3); however a two-layered model cannot be ruled out.

Backazimuthal variations in splitting at station RES are modelled as arising from two layers of anisotropy, with an upper-layer fast-polarisation orientation of 90–105° and a lower layer of ~30°. We compare the upper layer orientation with tectonic trends, assuming vertically-coherent lithospheric deformation; however these trends are difficult to decipher since the tectonic boundaries of the crystalline basement are obscured by Devonian—Cretaceous sedimentary basin sequences. Magnetic anomaly strikes may provide some information if such anomalies represent tectonic boundaries that persist through the crust and into the mantle lithosphere. Magnetic anomaly data are sparse in this region; however some recent maps (Gaina et al., 2011) show broadly E-W trending anomalies close to RES, cross-cutting the N-S trending Boothia structures.

While horizontal compressive stress may play a role in upper-crustal anisotropy, the resulting delay times would be too small to explain our observations and models for the upper layer of anisotropy at station RES. Near-surface anisotropy arising from such stress is of order ~10%, decreasing rapidly with depth (e.g. Boness and Zoback, 2006, and references therein). A 5 km thick layer with 10% anisotropy would only contribute 0.15 s to the delay time, for example, whereas Fig. 6 shows that the average delay time at RES is ~1 s. A more likely candidate remains mineral alignment in the lower crust and upper mantle, associated with the deformational history of the region. The High Arctic has a complex tectonic history with multiple phases of orogeny and extension (e.g. Piepjohn et al., 2016), which could give rise to a series of structural and mineralogical alignments preserved as anisotropic fabric in the lithosphere.

Mantle flow models (e.g. Forte et al., 2015) suggest a roughly NE-SW to ENE-WSW direction for mantle convective flow beneath the region, in contrast to the NNE/NE–SSW/SW orientation of the lower layer of splitting. However, such models assume a uniform lithospheric thickness at a global scale. Local thinning of the lithosphere as suggested by tomographic models (Schaeffer and Lebedev, 2014; Lebedev et al., 2018) may act to deflect mantle flow at a local to regional scale, therefore sublithospheric mantle convective flow remains a possible interpretation of the lower layer. The fast-polarisation orientation is also consistent with the orientation of azimuthal anisotropy at depths of ~150–330 km in the tomographic model of Schaeffer et al. (2016), for which the isotropic component (Schaeffer and Lebedev, 2013) images the local lithospheric thinning beneath the region surrounding RES.

5.6. Contributions from lower-mantle anisotropy

At station ALE, there is clear evidence for a systematic discrepancy between SKS and SKKS splitting characteristics for events arriving from the backazimuth range ~290–310°. An earlier shear wave splitting study by Niu and Perez (2004), using a global data set, also noted SKS/SKKS discrepancies at station ALE from a set of 3 measurements made at the same WNW–NW backazimuth range. The earthquakes from which these measurements were made are located in the Tonga-Fiji subduction system. We calculated the piercing points for SKS and SKKS phases ascending through the lowermost mantle at a depth of 2800 km, using the TauP Toolkit (Crotwell et al., 1999), and found that the two sets of piercing points were separated by ~1400 km laterally, with the SKS piercing points located beneath the Canada Basin of the Arctic Ocean and the SKKS piercing points located beneath northern Alaska and northwesternmost Russia (Supplementary Material, Fig. S3). Alaska has previously been noted as a zone of lowermost-mantle anisotropy using a variety of techniques including shear wave splitting and differential travel times for S, Sdiff and ScS phases (Restivo and Helffrich, 2006; Nowacki et al., 2011, and references therein).

6. Conclusions

We have used a combination of data from long-term / permanent and short-term seismograph installations to study the seismic anisotropy beneath the Canadian High Arctic. In general, the majority of the shear wave splitting measurements exhibit fast-polarisation orientations parallel or subparallel to the major tectonic trends and boundaries visible in surface geology and potential-field data. This, in addition to the significant variation in fast-polarisation orientation between some closely-spaced stations, suggests that the dominant source of the anisotropy is related to lithospheric structural alignments, i.e. a "fossil" deformation signature. The lithosphere of the High Arctic region is sufficiently thick to explain most, if not all, of the XKS delay times, assuming a plausible anisotropic strength for olivine-dominated lattice-preferred orientation. However, partial correlation with the modelled directions of present-day sublithospheric flow indicates that this flow cannot be ruled out as a secondary source of anisotropy.

Station RES, in the central Canadian Arctic, exhibits significant variation in splitting parameters as a function of event backazimuth. The pattern of variation can be explained by a simple model of two horizontal anisotropic layers. The upper layer has a roughly E–W fast-polarisation orientation (90–105°) whereas the lower layer is orientated approximately NNE–SSW (~30°). Although tectonic trends are difficult to decipher in this region, magnetic anomaly data suggest the presence of E–W trending structures, and models of geopotential stress at lithospheric depths show a similar orientation. The lower layer is subparallel to inferred sublithospheric mantle flow and may represent a region where the lithosphere is sufficiently thin to allow such flow to make a contribution to the observed splitting measurements.

A systematic discrepancy is observed between SKS and SKKS measurements from the NW quadrant at station ALE (northern Ellesmere Island). The most likely source of this anomaly, based on analysis of source-to-station ray paths, is a zone of anisotropy in the lowermost mantle beneath northwestern Alaska and the Chukchi Sea.

Data availability

Data from the ELLITE stations and some of the long-term stations (Scripps Inst. Oceanography, 1986; Stephenson et al., 2013) are available through the IRIS Data Management Center; the remaining

Canadian data are available through the Canadian National Data Centre, Natural Resources Canada (Geological Survey of Canada, 1989). Details are given via the following URLs: (1) www.fdsn.org/networks/detail/1E_2010/ (ELLITE), (2) www.fdsn.org/networks/detail/CN/ (Canadian National Seismograph Network), (3) www.fdsn.org/networks/detail/II/ (Global Seismograph Network).

Declaration of Competing Interest

The authors declare that they have no known competing financial interests or personal relationships that could have appeared to influence the work reported in this paper.

Appendix A. Supplementary data

Supplementary data to this article can be found online at https://doi.org/10.1016/j.tecto.2020.228524.

References

Alsina, D., Snieder, R., 1995. Small-scale sublithospheric continental mantle deformation: constraints from SKS splitting observations. Geophys. J. Int. 123, 431–448. https://doi.org/10.1111/j.1365-246X.1995.tb06864.x.
Argus, D., Gordon, R., Heflin, M., Ma, C., Eanes, R., Willis, P., Peltier, W., Owen, S., 2010. The angular velocities of the plates and the velocity of Earth's Centre from space geodesy. Geophys. J. Int. 180, 913–960. https://doi.org/10.1111/j.1365-246X.2009.04463.x.
Argyle, M., Forsyth, D., 1994. Interpretation of data and presentation of results from the Ice Island 1986 and 1990 seismic refraction experiments. Geol. Surv. Can. Open File 2973. https://doi.org/10.4095/194781.
Asudeh, I, Forsyth, D., Stephenson, R., Embry, A., Jackson, H., White, D., 1989. Crustal structure of the Canadian polar margin: results of the 1985 seismic refraction survey. Can. J. Earth Sci. 26, 853–866. https://doi.org/10.1139/e89-069.
Barruol, G., Mainprice, D., 1993. A quantitative evaluation of the contribution of crustal rocks to the shear-wave splitting of teleseismic SKS waves. Phys. Earth Planet. Inter. 78, 281–300. https://doi.org/10.1016/0031-9201(93)90161-2.
Barruol, G., Helffrich, G., Vauchez, A., 1997. Shear wave splitting around the northern Atlantic: frozen Pangaean lithospheric anisotropy? Tectonophysics 279, 135–148. https://doi.org/10.1016/S0040-1951(97)00126-1.
Bastow, I., Owens, T., Helffrich, G., Knapp, J., 2007. Spatial and temporal constraints on sources of seismic anisotropy: evidence from the Scottish highlands. Geophys. Res. Lett. 34. https://doi.org/10.1029/2006GL028911.
Bastow, I., Thompson, D., Kendall, J.M., Helffrich, G., Wookey, J., Snyder, D., Eaton, D., Darbyshire, F., 2011. Precambrian plate tectonics: seismic evidence from Northern Hudson Bay. Geology 39, 91–94. https://doi.org/10.1130/G31396.1.
Becker, T., Lebedev, S., Long, M., 2012. On the relationship between azimuthal anisotropy from shear wave splitting and surface wave tomography. J. Geophys. Res. 117. https://doi.org/10.1029/2011JB008705.
Bedle, H., van der Lee, S., 2009. S velocity variations beneath North America. J. Geophys. Res. 114, 53–68. https://doi.org/10.1029/2008JB005949.
Ben-Ismail, W., Barruol, G., Mainprice, D., 2001. The Kaapvaal craton seismic anisotropy: petrophysical analyses of upper mantle kimberlite nodules. Geophys. Res. Lett. 28, 2497–2500. https://doi.org/10.1029/2000GL012419.
Bokelmann, G.H., Wüstefeld, A., 2009. Comparing crustal and mantle fabric from the north American craton using magnetics and seismic anisotropy. Earth Planet. Sci. Lett. 277, 355–364. https://doi.org/10.1016/j.epsl.2008.10.032.

Boness, N.L., Zoback, M.D., 2006. Mapping stress and structurally controlled crustal shear velocity anisotropy in California. Geology 34, 825–828. https://doi.org/10.1130/G22309.1.
Bostock, M., Cassidy, J., 1995. Variations in SKS splitting across western Canada. Geophys. Res. Lett. 22, 5–8. https://doi.org/10.1029/94GL02789.
Brune, J., Dorman, J., 1963. Seismic waves and earth structure in the Canadian Shield. Bull. Seismol. Soc. Am. 53, 167–210.
Buchbinder, G., 1963. Crustal structure in Arctic Canada from Rayleigh waves. Trans. R. Soc. Can. 1, 333–355.
Bystricky, M., Kunze, K., Burlini, L., Burg, J.P., 2000. High shear strain of olivine aggregates: Rheological and seismic consequences. Science 290, 1564–1567. https://doi.org/10.1126/science.290.5496.1564.
Conrad, C.P., Behn, M.D., Silver, P.G., 2007. Global mantle flow and the development of seismic anisotropy: differences between the oceanic and continental upper mantle. J. Geophys. Res. 112. https://doi.org/10.1029/2006JB004608.
Crotwell, H.P., Owens, T., Ritsema, J., 1999. The TauP Toolkit: Flexible Seismic Travel-time and Ray-path Utilities. Seismol. Res. Lett. 70, 154–160.
Dahl-Jensen, T., Larsen, T.B., Woelbern, I., Bach, T., Hanka, W., Kind, R., Gregersen, S., Mosegaard, K., Voss, P., Gudmundsson, O., 2003. Depth to Moho in Greenland: receiver-function analysis suggests two Proterozoic blocks in Greenland. Earth Planet. Sci. Lett. 205, 379–393. https://doi.org/10.1016/S0012-821X(02)01080-4.
Darbyshire, F.A., 2003. Crustal structure across the Canadian High Arctic region from teleseismic receiver function analysis. Geophys. J. Int. 152, 372–391. https://doi.org/10.1046/j.1365-246X.2003.01840.x.
Darbyshire, F., 2005. Upper mantle structure of Arctic Canada from Rayleigh wave dispersion. Tectonophysics 405, 1–23. https://doi.org/10.1016/j.tecto.2005.02.013.
Debayle, E., Ricard, Y., 2013. Seismic observations of large-scale deformation at the bottom of fast-moving plates. Earth Planet. Sci. Lett. 376, 165–177. https://doi.org/10.1016/j.epsl.2013.06.02.
Embry, A., Beauchamp, B., 2008. Sverdrup Basin, in: Miall, A. (Ed.), Sedimentary Basins of the World:, 5 The Sedimentary Basins of the United States and Canada. Elsevier, Amsterdam, pp. 451–471.
Evans, M., Kendall, J.M., Willemann, R., 2006. Automated SKS splitting and upper-mantle anisotropy beneath Canadian seismic stations. Geophys. J. Int. 165, 931–942. https://doi.org/10.1111/j.1365-246X.2006.02973.x.
Forsyth, D., Mair, J., Fraser, I., 1979. Crustal structure of the Central Sverdrup Basin. Can. J. Earth Sci. 16, 1581–1598. https://doi.org/10.1139/e79-144.
Forsyth, D., Argyle, M., Okulitch, A., Trettin, H., 1994. New seismic, magnetic, and gravity constraints on the crustal structure of the Lincoln Sea continent–ocean transition. Can. J. Earth Sci. 31, 905–918. https://doi.org/10.1139/e94-082.
Forsyth, D., Asudeh, I., White, D., Jackson, R., Stephenson, R., Embry, A., Argyle, M., 1998. Sedimentary basins and basement highs beneath the polar shelf north of Axel Heiberg and Meighen islands. Bull. Can. Petrol. Geol. 46, 12–29.
Forte, A., Moucha, R., Simmons, N., Grand, S., Mitrovica, J., 2010. Deep-mantle contributions to the surface dynamics of the north American continent. Tectonophysics 481, 3–15. https://doi.org/10.1016/j.tecto.2009.06.010.
Forte, A., Simmons, N., Grand, S., 2015. Constraints on Seismic Models from Other Disciplines - Constraints on 3-D Seismic Models from Global Geodynamic Observables: Implications for the Global Mantle Convective Flow, in: Romanowicz, B., Dziewonski, A. (Eds.), Treatise of Geophysics, 2nd Edition, pp. 853–907. https://doi.org/10.1016/B978-0-444-53802-4.00028-2.
Funck, T., Jackson, H.R., Dehler, S.A., Reid, I.D., 2006. A refraction seismic transect from Greenland to Ellesmere Island, Canada: the crustal structure in southern Nares Strait. Polarforschung 74, 97–112.
Funck, T., Jackson, H.R., Shimeld, J., 2011. The crustal structure of the Alpha Ridge at the transition to the Canadian Polar margin: results from a seismic refraction experiment. J. Geophys. Res. 116. https://doi.org/10.1029/2011JB008411.
Gaina, C., Werner, S.C., Saltus, R., Maus, S., et al., 2011. Circum-Arctic mapping project: new magnetic and gravity anomaly maps of the Arctic. Geol. Soc. Lond. Mem. 35, 39–48. https://doi.org/10.1144/M35.3.
Gaina, C., Medvedev, S., Torsvik, T.H., Koulakov, I., Werner, S.C., 2014. 4D Arctic: a Glimpse into the Structure and Evolution of the Arctic in the Light of New Geophysical Maps, Plate Tectonics and Tomographic models. Surv. Geophys. 35, 1095–1122. https://doi.org/10.1007/s10712-013-9254-y.
Geological Survey of Canada, 1989. Canadian National Seismograph Network. International Federation of Digital Seismograph Networks https://doi.org/10.7914/SN/CN. Dataset/Seismic Network.
Gripp, A., Gordon, R., 2002. Young tracks of hotspots and current plate velocities. Geophys. J. Int. 150, 321–361. https://doi.org/10.1046/j.1365-246X.2002.01627.x.
Hadlari, T., Davis, W., Dewing, K., 2014. A pericratonic model for the Pearya terrane as an extension of the Franklinian margin of Laurentia, Canadian Arctic. Geol. Soc. Am. Bull. 126, 182–200. https://doi.org/10.1130/B30843.1.
Hammond, J.O., Kendall, J.M., Rümpker, G., Wookey, J., Teanby, N., Joseph, P., Ryberg, T., Stuart, G., 2005. Upper mantle anisotropy beneath the Seychelles microcontinent. J. Geophys. Res. 110. https://doi.org/10.1029/2005JB003757.
Harrison, J., St-Onge, M., Petrov, O., Strelnikov, S., Lopatin, B., Wilson, F., Tella, S., Paul, D., Lynds, T., Shokalsky, S., Hults, C., Bergman, S., Jepsen, H., Solli, A., 2011. Geological map of the Arctic. Geol. Surv. Canada Map 2159A (scale 1:5000000).
Helffrich, G., 1995. Lithospheric deformation inferred from teleseismic shear wave splitting observations in the United Kingdom. J. Geophys. Res. 100, 18195–18204. https://doi.org/10.1029/95JB01572.
Helffrich, G., Silver, P., Given, H., 1994. Shear-wave splitting variation over short spatial scales on continents. Geophys. J. Int. 119, 561–573. https://doi.org/10.1111/j.1365-246X.1994.tb00142.x.
Jackson, H.R., Reid, I., 1994. Crustal thickness variations between the Greenland and Ellesmere Island margins determined from seismic refraction. Can. J. Earth Sci. 31,

1407–1418. https://doi.org/10.1139/e94-124.

Jackson, H., Keen, C., Barrett, D., 1977. Geophysical studies on the eastern continental margin of Baffin Bay and in Lancaster Sound. Can. J. Earth Sci. 14, 1991–2001. https://doi.org/10.1139/e77-170.

Jackson, H., Marillier, F., Hall, J., 1998. Seismic refraction data in the Gulf of Saint Lawrence: implications for the lower-crustal blocks. Can. J. Earth Sci. 35, 1222–1237. https://doi.org/10.1139/e98-043.

Jenkins, J., Deuss, A., Cottaar, S., 2017. Converted phases from sharp 1000 km depth mid-mantle heterogeneity beneath Western Europe. Earth Planet. Sci. Lett. 459, 196–207. https://doi.org/10.1016/j.epsl.2016.11.031.

Kaminski, É., Ribe, N.M., 2002. Timescales for the evolution of seismic anisotropy in mantle flow. Geochem. Geophys. Geosyst. 3, 1–17. https://doi.org/10.1029/2001GC000222.

Keen, C., Barrett, D., Manchester, K., Ross, D., 1972. Geophysical studies in Baffin Bay and some tectonic implications. Can. J. Earth Sci. 9, 239–256. https://doi.org/10.1139/e72-020.

Kennett, B., Engdahl, E., 1991. Travel times for global earthquake location and phase association. Geophys. J. Int. 105, 429–465. https://doi.org/10.1111/j.1365-246X.1991.tb06724.x.

Lebedev, S., Schaeffer, A.J., Fullea, J., Pease, V., 2018. Seismic tomography of the Arctic region: inferences for the thermal structure and evolution of the lithosphere. Geol. Soc. London. Spec. Pub. 460, 419–440. https://doi.org/10.1144/SP460.10.

Liddell, M.V., Bastow, I., Darbyshire, F., Gilligan, A., Pugh, S., 2017. The formation of Laurentia: evidence from shear wave splitting. Earth Planet. Sci. Lett. 479, 170–178. https://doi.org/10.1016/j.epsl.2017.09.030.

Long, M.D., Jackson, K.G., McNamara, J.F., 2016. SKS splitting beneath Transportable Array stations in eastern North America and the signature of past lithospheric deformation. Geochem. Geophys. Geosyst. 17, 2–15. https://doi.org/10.1002/2015GC006088.

Mitrovica, J., Forte, A., 2004. A new inference of mantle viscosity based upon joint inversion of convection and glacial isostatic adjustment data. Earth Planet. Sci. Lett. 225, 177–189. https://doi.org/10.1016/j.epsl.2004.06.005.

Niu, F., Perez, A.M., 2004. Seismic anisotropy in the lower mantle: a comparison of waveform splitting of SKS and SKKS. Geophys. Res. Lett. 31. https://doi.org/10.1029/2004GL021196.

Nowacki, A., Wookey, J., Kendall, J.M., 2011. New advances in using seismic anisotropy, mineral physics and geodynamics to understand deformation in the lowermost mantle. J. Geodyn. 52, 205–228. https://doi.org/10.1016/j.jog.2011.04.003.

Oakey, G.N., Chalmers, J.A., 2012. A new model for the Paleogene motion of Greenland relative to North America: plate reconstructions of the Davis Strait and Nares Strait regions between Canada and Greenland. J. Geophys. Res. 117. https://doi.org/10.1029/2011JB008942.

Oakey, G.N., Stephenson, R., 2008. Crustal structure of the Innuitian region of Arctic Canada and Greenland from gravity modelling: implications for the Palaeogene Eurekan orogen. Geophys. J. Int. 173, 1039–1063. https://doi.org/10.1111/j.1365-246X.2008.03784.x.

Pease, V., Drachev, S., Stephenson, R., Zhang, X., 2014. Arctic lithosphere—a review. Tectonophysics 628, 1–25. https://doi.org/10.1016/j.tecto.2014.05.033.

Petrov, O., Morozov, A., Shokalsky, S., Kashubin, S., Artemieva, I.M., Sobolev, N., Petrov, E., Ernst, R.E., Sergeev, S., Smelror, M., 2016. Crustal structure and tectonic model of the Arctic region. Earth Sci. Rev. 154, 29–71. https://doi.org/10.1016/j.earscirev.2015.11.013.

Piepjohn, K., von Gosen, W., 2018. Structural transect through Ellesmere Island (Canadian Arctic): superimposed Palaeozoic Ellesmerian and Cenozoic Eurekan deformation. Geol. Soc. London. Spec. Pub. 460, 33–56. https://doi.org/10.1144/SP460.5.

Piepjohn, K., von Gosen, W., Tessensohn, F., 2016. The Eurekan deformation in the Arctic: an outline. J. Geol. Soc. 173, 1007–1024. https://doi.org/10.1144/jgs2016-081.

Reid, I., Jackson, H., 1997. Crustal structure of northern Baffin Bay: Seismic refraction results and tectonic implications. J. Geophys. Res. 102, 523–542. https://doi.org/10.1029/96JB02656.

Restivo, A., Helffrich, G., 1999. Teleseismic shear wave splitting measurements in noisy environments. Geophys. J. Int. 137, 821–830. https://doi.org/10.1046/j.1365-246x.1999.00845.x.

Restivo, A., Helffrich, G., 2006. Core–mantle boundary structure investigated using SKS and SKKS polarization anomalies. Geophys. J. Int. 165, 288–302. https://doi.org/10.1111/j.1365-246X.2006.02901.x.

Savage, M., 1999. Seismic anisotropy and mantle deformation: what have we learned from shear wave splitting. Rev. Geophys. 37, 65–106. https://doi.org/10.1029/98RG02075.

Schaeffer, A., Lebedev, S., 2013. Global shear speed structure of the upper mantle and

transition zone. Geophys. J. Int. 194, 417–449. https://doi.org/10.1093/gji/ggt095.

Schaeffer, A., Lebedev, S., 2014. Imaging the north American continent using waveform inversion of global and USArray data. Earth Planet. Sci. Lett. 402, 26–41. https://doi.org/10.1016/j.epsl.2014.05.014.

Schaeffer, A., Lebedev, S., Becker, T., 2016. Azimuthal seismic anisotropy in the Earth's upper mantle and the thickness of tectonic plates. Geophys. J. Int. 207, 901–933. https://doi.org/10.1093/gji/ggw309.

Schiffer, C., Stephenson, R., 2018. Regional crustal architecture of Ellesmere Island, Arctic Canada. Geol. Soc. London. Spec. Pub. 460, 19–32. https://doi.org/10.1144/SP460.8.

Schiffer, C., Stephenson, R., Oakey, G.N., Jacobsen, B.H., 2016. The crustal structure of Ellesmere Island, Arctic Canada—teleseismic mapping across a remote intraplate orogenic belt. Geophys. J. Int. 204, 1579–1600. https://doi.org/10.1093/gji/ggv539.

Scripps Inst. Oceanography, 1986. IRIS/IDA Seismic Network. International Federation of Digital Seismograph Networks https://doi.org/10.7914/SN/II. Dataset/Seismic Network.

Silver, P., 1996. Seismic anisotropy beneath the continents: probing the depths of geology. Annu. Rev. Earth Planet. Sci. 24, 385–432. https://doi.org/10.1146/annurev.earth.24.1.385.

Silver, P., Chan, W., 1988. Implications for continental structure and evolution from seismic anisotropy. Nature 335, 34–39. https://doi.org/10.1038/335034a0.

Silver, P.G., Chan, W.W., 1991. Shear wave splitting and subcontinental mantle deformation. J. Geophys. Res. 96, 16,429–16,454. https://doi.org/10.1029/91JB00899.

Silver, P., Savage, M., 1994. The interpretation of shear wave splitting parameters in the presence of two anisotropic layers. Geophys. J. Int. 119, 949–963. https://doi.org/10.1111/j.1365-246X.1994.tb04027.x.

Stephenson, R., Oakey, G., Schiffer, C., Jacobsen, B., 2013. Ellesmere Island Lithosphere Experiment (ELLITE): Eurekan basin inversion and mountain building, Ellesmere Island, Nunavut. Geol. Surv. Can. Curr. Res. 2013-21 https://doi.org/10.4095/292859. 8pp.

Stephenson, R., Piepjohn, K., Schiffer, C., Von Gosen, W., Oakey, G.N., Anudu, G., 2018. Integrated crustal–geological cross-section of Ellesmere Island. Geol. Soc. London. Spec. Pub. 460, 7–17. https://doi.org/10.1144/SP460.12.

St-Onge, M., Harrison, J., Paul, D., Tella, S., Brent, T., Jauer, C., Maclean, B., 2015. Tectonic map of Arctic Canada, Geological Survey of Canada, Canadian Geoscience Map 187 (preliminary), scale 1:4000000. https://doi.org/10.4095/295945.

Teanby, N., Kendall, J.M., Van der Baan, M., 2004. Automation of shear-wave splitting measurements using cluster analysis. Bull. Seismol. Soc. Am. 94, 453–463. https://doi.org/10.1785/0120030123.

Tommasi, A., Mainprice, D., Canova, G., Chastel, Y., 2000. Viscoplastic self-consistent and equilibrium-based modeling of olivine lattice preferred orientations: Implications for the upper mantle seismic anisotropy. J. Geophys. Res. 105, 7893–7908. https://doi.org/10.1029/1999JB900411.

Trettin, H., Okulitch, A., Harrison, J., Brent, T., Fox, F., Packard, J., Smith, G., Zolnai, A., 1991. Silurian - Early Carboniferous deformational phases and associated metamorphism and plutonism, Arctic Islands, in: Trettin, H. (Ed.), Geology of the Innuitian Orogen and Arctic Platform of Canada and Greenland: Geology of Canada, 3. Geological Survey of Canada, pp. 293–341.

Walker, A.M., Wookey, J., 2012. MSAT - a new toolkit for the analysis of elastic and seismic anisotropy. Comput. Geosci. 49, 81–90. https://doi.org/10.1016/j.cageo.2012.05.031.

Walpole, J., Wookey, J., Masters, G., Kendall, J., 2014. A uniformly processed data set of SKS shear wave splitting measurements: a global investigation of upper mantle anisotropy beneath seismic stations. Geochem. Geophys. Geosyst. 15, 1991–2010. https://doi.org/10.1002/2014GC005278.

Wickens, A., 1971. Variations in lithospheric thickness in Canada. Can. J. Earth Sci. 8, 1154–1162. https://doi.org/10.1139/e71-103.

Wickens, A., Pec, K., 1968. A crust-mantle profile from Mould Bay, Canada, to Tucson, Arizona. Bull. Seismol. Soc. Am. 58, 1821–1831.

Wolfe, C.J., Silver, P.G., 1998. Seismic anisotropy of oceanic upper mantle: Shear wave splitting methodologies and observations. J. Geophys. Res. 103, 749–771. https://doi.org/10.1029/97JB02023.

Yuan, K., Beghein, C., 2013. Seismic anisotropy changes across upper mantle phase transitions. Earth Planet. Sci. Lett. 374, 132–144. https://doi.org/10.1016/j.epsl.2013.05.031.

Yuan, H., Romanowicz, B., Fischer, K., Abt, D., 2011. 3-D shear wave radially and azimuthally anisotropic velocity model of the north American upper mantle. Geophys. J. Int. 184, 1237–1260. https://doi.org/10.1111/j.1365-246X.2010.040901.x.

Zhang, S., Karato, S.I., 1995. Lattice preferred orientation of olivine aggregates deformed in simple shear. Nature 375, 774–777. https://doi.org/10.1038/375774a0.